

Geometrical confinement effects in layered mesoscopic vortex-matter

N. R. Cejas Bolecek,¹ M. I. Dolz,² A. Kolton,³ H. Pastoriza,¹ C. J. van der Beek,⁴ M. Konczykowski,⁴ M. Menghini,⁵ G. Nieva,¹ and Y. Fasano¹

¹*Low Temperature Division, Centro Atómico Bariloche, CNEA, Argentina*

²*Universidad Nacional de San Luis, San Luis, Argentina*

³*Solid State Theory group, Centro Atómico Bariloche, CNEA, Argentina*

⁴*Laboratoire des Solides Irradiés, Ecole Polytechnique, Palaiseau, France*

⁵*Katholieke Universitat Leuven, Leuven, Belgium*

(Dated: September 26, 2014)

We study geometrical confinement effects in $\text{Bi}_2\text{Sr}_2\text{CaCu}_2\text{O}_{8+\delta}$ mesoscopic vortex-matter with edge-to-surface ratio of 7 – 12%. Samples have in-plane square and circular edges, $30\ \mu\text{m}$ widths, and $\sim 2\ \mu\text{m}$ thickness. Direct vortex imaging reveals the compact planes of the structure align with the sample edge by introducing topological defects. The defects density is larger for circular than for square edges. Molecular dynamics simulations suggest this density is not an out-of-equilibrium property but rather determined by the geometrical confinement.

PACS numbers:

I. INTRODUCTION

Understanding the confinement effects introduced by sample geometry is crucial for characterizing the static and dynamic properties of mesoscopic vortex matter. This subject was actively investigated for low-temperature superconductors with dimensions comparable or smaller than coherence length or penetration depth, λ^{1-6} . Mesoscopic vortex matter in these materials have structural properties strongly influenced by the geometry of the specimens³, in contrast with results in macroscopic samples for several compounds⁷⁻¹⁰. Confinement effects are in competition with inter-vortex interaction that increases with field and temperature. Materials with an important electronic anisotropy such as layered high- T_c 's have quite a large value of λ and then inter-vortex interactions become more relevant.

Due to the technical difficulties for fabricating micron-sized samples of layered high- T_c 's complex oxides, there are few works in the literature investigating the effect of confinement in vortex matter nucleated in these materials¹¹. In this work we study this issue in the paradigmatic $\text{Bi}_2\text{Sr}_2\text{CaCu}_2\text{O}_{8+\delta}$ compound that presents a rich vortex phase diagram governed by thermal fluctuations and extremely anisotropic magnetic properties. In this compound, the phase diagram of macroscopic as well as mesoscopic²¹ vortex matter is dominated by a first-order transition^{12,13} between a solid phase at low temperatures and a liquid¹⁴ or decoupled gas^{15,16} of pancake vortices at high temperatures. The vortex solid phase of macroscopic samples presents quasi long-range positional order¹⁷.

Here we report on the structural properties of the mesoscopic vortex solid nucleated in $\text{Bi}_2\text{Sr}_2\text{CaCu}_2\text{O}_{8+\delta}$ at low fields and with single-vortex resolution. We study both, experimentally and with simulations, the effect of confinement and inter-vortex interactions for samples with square and circular edges experimental.

II. METHODS

We engineered micron-sized superconducting samples from bulk $\text{Bi}_2\text{Sr}_2\text{CaCu}_2\text{O}_{8+\delta}$ crystals ($T_c = 89\ \text{K}$). We fabricated circular and square samples with typical dimensions of $30\ \mu\text{m}$ by means of optical lithography and subsequent physical ion-milling of the negative of the samples¹⁸. Freestanding $2\ \mu\text{m}$ thick disks and cuboids are obtained after cleaving the towers resulting from milling.

We directly imaged the solid vortex phase with single-vortex resolution by means of magnetic decoration experiments performed at $4.2\ \text{K}$ after field-cooling¹⁹. In these experiments the evaporated magnetic nanoparticles land in the sample surface at the places where the gradient of local inductance is maximum, therefore decorating the vortex positions. The imaged structure corresponds to the vortex solid frozen at the temperature at which pinning sets in, $T_{\text{freeze}} \sim T_{\text{irr}}^7$, of the order of $90 - 87\ \text{K}$ for the low-fields studied here²⁰. Decreasing the sample size down to microns does not significantly affect the value of $T_{\text{irr}}^{\text{21}}$.

We also performed molecular dynamics simulations of two-dimensional vortex matter in order to emulate the experimentally-observed vortex matter structural properties²². We studied the case of $30\ \mu\text{m}$ diameter disks and focused on the density of topological defects when varying the simulation cooling-rate.

III. RESULTS AND DISCUSSION

Figure 1 shows snapshots of the mesoscopic vortex structure nucleated in the disk and cuboid $\text{Bi}_2\text{Sr}_2\text{CaCu}_2\text{O}_{8+\delta}$ samples after field-cooling down to $4.2\ \text{K}$ at applied fields of 20 and 40 Oe. The local induction calculated as the number of vortices times the flux quantum yields $B \sim 0.75H$, a reduction due to demagnetizing effects (aspect ratio of the disks and cuboids of ~ 15). The direction of the compact planes of the

vortex structure in micron-sized specimens is affected by the confinement effect introduced by the edges of the samples, particularly in the case of the outer shells of vortices. This finding is in contrast to observations in macroscopic samples⁷. The alignment is more evident in the Delaunay triangulations of Fig. 2, a well known geometrical algorithm that determines the first-neighbors for every vortex in the structure¹⁷. First-neighbors vortices are bounded with lines and non-sixfold coordinated ones are highlighted in grey. In the case of the cuboid samples, irrespective of the vortex density (447 *vs.* 1092), one of the compact planes of the structure is parallel to the sample edge. For the disks, only a few outer shells of vortices mimic the sample edges, the number depending inversely with the vortex density. Towards the center of the sample, a rather ordered vortex crystallite is formed with the compact planes having no register with the sample edges. The transition between the orientation of the outer and inner shells is done via the plastic deformations entailed by topological defects.

For the vortex structure studied here these topological defects are generally disclinations, namely vortices with five or seven first-neighbors, and pairs of them or screw-dislocations associated to an extra plane of vortices. For example, isolated dislocations are observed in the middle of the vortex structure nucleated in the cuboid at an

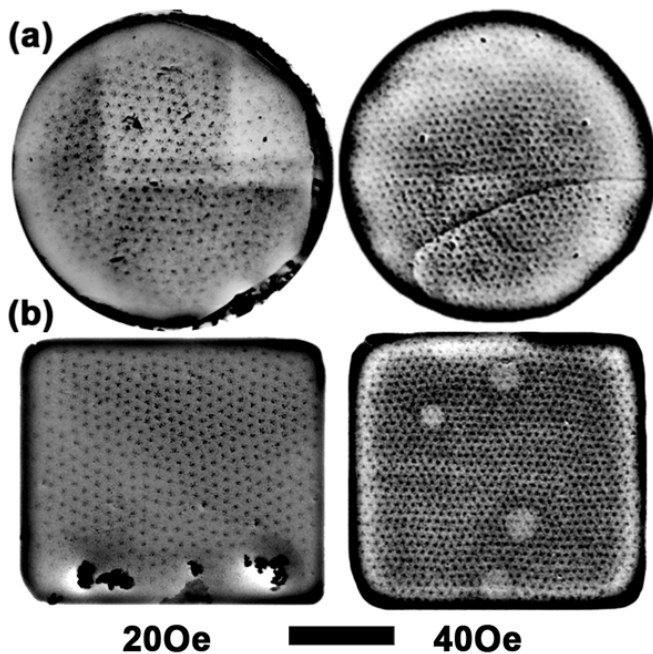


Figure 1: Magnetic decoration images of the mesoscopic vortex matter nucleated in field-cooling processes in micron-sized $\text{Bi}_2\text{Sr}_2\text{CaCu}_2\text{O}_{8+\delta}$ samples. (a) Disk with $30\ \mu\text{m}$ diameter and (b) cuboid with $30\ \mu\text{m}$ sides length, all samples with $2\ \mu\text{m}$ thickness. Magnetic decorations were performed at 4.2K and at applied fields of 20 (left panel) and 40 Oe (right panel). The scale-bar corresponds to $10\ \mu\text{m}$.

applied field of 40 Oe. The density of non-sixfold coordinated vortices, ρ_{def} , strongly depends on the local induction. In the case of macroscopic $\text{Bi}_2\text{Sr}_2\text{CaCu}_2\text{O}_{8+\delta}$ vortex matter, ρ_{def} decreases exponentially up to 20 Gauss and then saturates around 2% as shown in Fig. 3 (a). This is due to the enhancement of inter-vortex interaction on increasing field. This magnitude follows the same B -evolution for mesoscopic vortex matter but is at least 50% larger than for bulk samples. In addition, ρ_{def} is always larger in disks than in cuboids for roughly the same vortex density. This can be explained by considering that aligning a compact plane of vortices with the edges of a cuboid does not imply to change the orientational order of the structure whereas in order to do so in a disk the vortex planes have to bend.

In the case of macroscopic samples, it has been proved that the structure observed by means of field-cooling decorations at 4.2K, and therefore its ρ_{def} , is quite close to the equilibrium¹⁷. The possibility of the increase on the ρ_{def} on decreasing the system size being an out-of-equilibrium phenomena can not be discarded. Therefore we performed molecular dynamics simulations of the mesoscopic vortex matter nucleated in a $30\ \mu\text{m}$ disk with a density of 15 Gauss in order to test this possibility. In particular, we performed tests on the dependence of ρ_{def} with the cooling rate, inversely proportional to the time allowed to the system to relax. First, we performed simulations in a macroscopic sample in order to find the pinning magnitude that has to be considered in order to reproduce the observed ρ_{def} . Then we used this magni-

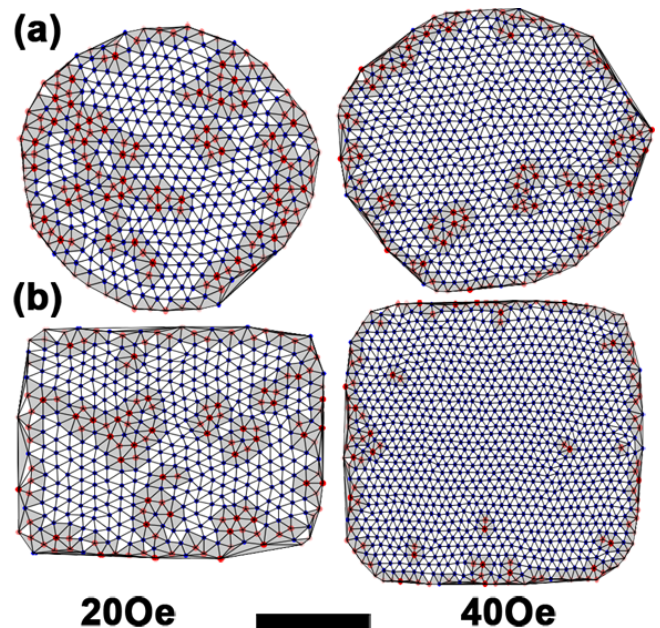


Figure 2: Delaunay triangulations of the mesoscopic vortex matter shown in Fig. 1. Disclinations are highlighted in gray; sixfold(non-sixfold)-coordinated vortices are indicated in blue(red). The scale-bar corresponds to $10\ \mu\text{m}$.

tude of pinning to perform simulations in micron-sized samples. The results of ρ_{def} as a function of the cooling rate, see Fig. 3 (b), indicate that the observed experimental values correspond to the case of large relaxation times. Therefore, we can ascertain that the amount of topological defects observed in the experiments in micron-sized samples is not an out-of-equilibrium feature and that the observed structure is quite close to the equilibrium.

Having this certainty in mind, we tried to estimate the geometrical confinement energy induced by the sample edges. In the case of bulk samples, the mean value of the inter-vortex interaction energy distribution is slightly shifted upward with respect to the value for a perfect Abrikosov lattice with the same vortex density¹⁰. Since after a field-cooling process vortices are close to equilibrium, this shifting can only be accounted by the effect of bulk pinning¹⁰. This can be expressed, by unit length, as $\langle \epsilon_{\text{int}} \rangle^{\text{b}} - \epsilon_{\text{Abr}} = \epsilon_{\text{p}}^{\text{b}}$, where b stands for the bulk sample and $\langle \epsilon_{\text{int}} \rangle$ is the mean value of a distribution of inter-vortex interaction energies, ϵ_{Abr} the value of the inter-vortex interaction energy in a perfect Abrikosov lattice (a delta-function), and ϵ_{p} the pinning energy. In the case of mesoscopic vortex matter, an extra term enters into the energy-balance, namely the confinement energy ϵ_{conf} and therefore $\langle \epsilon_{\text{int}} \rangle^{\text{meso}} - \epsilon_{\text{Abr}} = \epsilon_{\text{p}}^{\text{meso}} + \epsilon_{\text{conf}}$, where meso means for the case of mesoscopic vortex matter and the energies are noted similarly as in the previous case. Therefore, one can have access to an estimation of the confinement energy in mesoscopic vortex matter just by assuming that the pinning magnitude is the same irrespective of the sample size, and then $\epsilon_{\text{conf}} = \langle \epsilon_{\text{int}} \rangle^{\text{meso}} - \langle \epsilon_{\text{int}} \rangle^{\text{b}}$.

The inter-vortex interaction energy per unit length depends on the inter-vortex distances r_{ij} , and for a vortex i has a value $\epsilon_{\text{int}}^i = \sum_j 2\epsilon_0 K_0(r_{ij}/\lambda)$, with the sum over neighbor-vortices j , $\epsilon_0 \propto \lambda^2$ the vortex line ten-

sion, and K_0 the zeroth-order modified Bessel function. In real cases this magnitude is spatially inhomogeneous due to the elastic and plastic deformations of the structure, and therefore there is a distribution of ϵ_{int}^i with an almost-Gaussian shape¹⁰. Only in the case of an ideal Abrikosov lattice this magnitude is space invariant and its distribution is a delta function. We have performed inter-vortex energy-distribution calculations in vortex structures observed by magnetic decoration in the macroscopic samples from which were engineered the disks and cuboids. We also performed the same calculations in the mesoscopic vortex matter nucleated in the disks and cuboids at both applied fields. Irrespective of the field, the mean values of $\langle \epsilon_{\text{int}} \rangle^{\text{meso}}$ are always larger than in the case of macroscopic vortex matter, what can be reasonably ascribed to the extra deformations introduced by the larger amount of topological defects nucleated in the micron-sized samples. In accordance with this reasoning, the $\langle \epsilon_{\text{int}} \rangle^{\text{meso}}$ value is always larger for the structure nucleated in the disks than in the cuboids by a 6-9% on increasing field. Therefore the estimated confinement energy is in the case of disks equal to $1 \pm 0.1 \times 10^{-8} \text{ erg/cm} \sim 0.13\epsilon_0$, larger than in the case of cuboids, $0.8 \pm 0.1 \times 10^{-8} \text{ erg/cm} \sim 0.11\epsilon_0$.

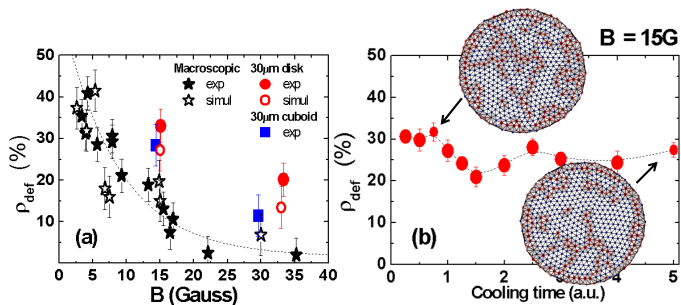


Figure 3: Density of topological defects (non-sixfold coordinated vortices) in mesoscopic and macroscopic $\text{Bi}_2\text{Sr}_2\text{CaCu}_2\text{O}_{8+\delta}$ vortex matter. (a) Experimental data as a function of applied field for the mesoscopic vortex structures nucleated in the 30 μm disk and cuboid, and macroscopic vortex matter. (b) Results from molecular dynamics simulations as a function of the simulations relaxation time in the case of a 30 μm disk and $B = 15$ Gauss.

IV. CONCLUSIONS

The edges of the samples do produce a geometrical confinement effect in mesoscopic vortex matter that is put in evidence by the orientation of the outer shells of vortices with compact planes parallel to the edges what produces a concomitant increase of the density of topological defects. By means of molecular dynamics simulations we show that the density of defects found experimentally is not an out-of-equilibrium feature but rather the effect introduced by geometrical confinement. By means of differences in the mean value of the inter-vortex interaction of the mesoscopic and macroscopic vortex structures we are able to quantify the confinement energy per unit length. We find that is just $0.11 - 0.13\epsilon_0$, the larger value in the case of disks than cuboid geometries.

-
- ¹ V. V. Moshchalkov, *et al.*, Nature **373**, 319 (1995).
² A. K. Geim, *et al.*, Nature **390**, 256 (1997).
³ V. A. Schweigert, F. M. Peeters, and P. S. Deo, Phys. Rev. Lett. **81**, 2783 (1998).
⁴ J. J. Palacios, Phys. Rev. B **58**, R5948 (1998).
⁵ V. Bruyndoncx, *et al.*, Phys. Rev. B **60**, 10468 (1999).
⁶ L. R. E. Cabral, B. J. Baelus, and F. M. Peeters, Phys. Rev. B **70**, 144523 (2004).
⁷ Y. Fasano, J. Herbsommer, and F. de la Cruz, Phys. Stat. Sol. (b) **215**, 563 (1999).
⁸ M. Menghini, *et al.*, Phys. Rev. Lett. **90**, 147001 (2003).
⁹ A. P. Petrovic, *et al.*, Phys. Rev. Lett. **103**, 257001 (2009).
¹⁰ S. Demirdis, *et al.*, Phys. Rev. B **84**, 094517 (2011).
¹¹ Y. M. Wang, *et al.*, Phys. Rev. B **65**, 184506, (2002)
¹² H. Pastoriza, *et al.*, Phys. Rev. Lett. **72**, 2951 (1994).
¹³ E. Zeldov, *et al.*, Nature **375**, 373 (1995).
¹⁴ D. R. Nelson, Phys. Rev. Lett. **60**, 1973 (1988).
¹⁵ L. I. Glazman, and A. E. Koshelev, Phys. Rev. B **43**, 2835 (1991).
¹⁶ H. Pastoriza and P. H. Kes, Phys. Rev. Lett. **75**, 3525 (1995).
¹⁷ Y. Fasano, *et al.*, Proc. Nat. Acad. Sci. **102**, 3898 (2005).
¹⁸ M. I. Dolz, A. B. Kolton and H. Pastoriza, Phys. Rev. B **81**, 092502 (2010).
¹⁹ Y. Fasano, *et al.*, Solid State Commun. **128**, 51 (2003).
²⁰ M.I. Dolz, *et al.*, submitted to Phys. Rev. B, cond-mat:1212.4564. (2014).
²¹ M. Konczykowski, *et al.*, cond-mat: arXiv:1212.4564.
²² A. Kolton, D. Domínguez, and N. Grønbech-Jensen, Phys. Rev. Lett. **83**, 3061 (1999).